

PAPER

Magnetic properties of misch-metal partially substituted Nd–Fe–B magnets sintered by dual alloy method

To cite this article: Jie-Fu Xiong *et al* 2018 *Chinese Phys. B* **27** 077504

View the [article online](#) for updates and enhancements.

Related content

- [Influence of misch metal content on microstructure and magnetic properties of R–Fe–B magnets sintered by dual alloy method](#)
Rong-Xiang Shang, Jie-Fu Xiong, Dan Liu et al.
- [Anisotropic nanocomposite soft/hard multilayer magnets](#)
Wei Liu and Zhidong Zhang
- [Abnormal variation of magnetic properties with Ce content in \$\(\text{PrNdCe}\)_2\text{Fe}_{14}\text{B}\$ sintered magnets prepared by dual alloy method](#)
Xue-Feng Zhang, Jian-Ting Lan, Zhu-Bai Li et al.

Magnetic properties of misch-metal partially substituted Nd–Fe–B magnets sintered by dual alloy method*

Jie-Fu Xiong(熊杰夫)^{1,2}, Rong-Xiang Shang(商荣翔)^{1,2}, Yan-Li Liu(刘艳丽)^{1,2}, Xin Zhao(赵鑫)^{1,2},
Wen-Liang Zuo(左文亮)^{1,2}, Feng-Xia Hu(胡凤霞)^{1,2}, Ji-Rong Sun(孙继荣)^{1,2},
Tong-Yun Zhao(赵同云)^{1,2}, Ren-Jie Chen(陈仁杰)³, and Bao-Gen Shen(沈保根)^{1,2,†}

¹State Key Laboratory of Magnetism, Institute of Physics, Chinese Academy of Sciences, Beijing 100190, China,

²University of Chinese Academy of Sciences, Beijing 100049, China

³Key Laboratory of Magnetic Materials and Devices, Ningbo Institute of Materials Technology and Engineering, Chinese Academy of Sciences, Ningbo 315201, China

(Received 22 March 2018; revised manuscript received 14 April 2018; published online 25 June 2018)

The misch-metal (MM) partially substituted Nd–Fe–B sintered magnets were fabricated by the dual alloy method, and the crystal structure, microstructure, and magnetic properties were analyzed comprehensively. X-ray diffraction (XRD) reveals that the increasing content of the MM has an inconsiderable effect on the crystallographic alignment of the magnets. Grains of the two main phases are uniformly distributed, and slightly deteriorate on the grain boundary. Due to the diffusion between the adjacent grains, the MM substituted Nd–Fe–B magnets contain three types of components with different Ce/La concentrations. Moreover, the first-order reversal curve (FORC) diagram is introduced to analyze the magnetization reversal process, coercivity mechanism, and distribution of reversal field in magnetic samples. The analysis indicates that there are two major reversal components, corresponding to the two different main phases. The domain nucleation and growth are determined to be the leading mechanism in controlling the magnetization reversal processes of the magnets sintered by the dual alloy method.

Keywords: misch-metal, first order reversal curve, the dual alloy method, magnetization reversal process

PACS: 75.60.Ej, 75.60.Jk

DOI: 10.1088/1674-1056/27/7/077504

1. Introduction

Nd₂Fe₁₄B based magnets have been the most widely used permanent magnets since they were discovered due to their excellent permanent magnetic performance at room temperature, and the application fields including traction motors of hybrid electric vehicles, wind generators, and magnetic resonance imaging.^[1,2] In order to reduce the production costs more rationally and make rational use of rare earth resources, the partial substitution of misch-metal (MM) for Nd in Nd–Fe–B sintered magnets is thought to be an effective method to pursue high cost performance because of the inferior intrinsic properties and low cost of MM₂Fe₁₄B.^[3–6] It has been found that the magnetic properties deteriorate drastically when Nd is replaced by Ce/La homogeneously in the 2:14:1 phase lattice.^[5] Compared with the traditional single alloy method, the dual alloy method by mixing MM₂Fe₁₄B with Nd₂Fe₁₄B powders has an obvious advantage in preparing high abundant rare earth permanent magnets.^[6,7] Coercivity and magnetic properties were greatly improved in the magnets sintered by the dual alloy method. The mixing of two types of powders may give rise to distinctly different microstructures in sintered magnets, and the magnetic properties were sensitive

to the microstructure.^[8,9] Thus, it is necessary to know how the magnetic properties are improved in these magnets.

It is the exchange coupling, which may protect the MM₂Fe₁₄B phase against magnetization reversal since Nd₂Fe₁₄B possesses high magnetocrystalline anisotropy, that makes magnetization reversal in adjacent grains of different magnetic phases more uniform.^[8,10] To some extent, short-range exchange coupling existing between local grains has been considered to be harmful to the coercivity of the sintered magnets.^[11,12] The magnetization reversal process has a substantial impact on developing novel permanent materials, and it is essential to obtain good knowledge of the process, which may provide guidance for the promotion of the performance of magnets. The first-order reversal curve (FORC) technique, as was shown recently, is powerful in identifying the magnetic phase both qualitatively and quantitatively;^[13] it is very delicate to irreversible magnetization processes,^[14,15] and distributions of reversal field,^[16] and is quite suitable to the analysis of the magnetic reversal process.

In this work, the effects of misch-metal substitution on the room-temperature permanent magnetic properties and the microstructure were studied in MM partially substituted Nd–Fe–B magnets sintered by the dual alloy method. Grain align-

*Project supported by the National Natural Science Foundation of China (Grant No. 51590880), the National Key Research and Development Program of China (Grant Nos. 2014CB643702 and 2016YFB0700903), Key Research Program of the Chinese Academy of Sciences of China, and the Inner Mongolia Science and Technology Major Project of China 2016.

†Corresponding author. E-mail: shenbaogen@yeah.net

ment and phase constitution were determined by x-ray diffraction (XRD). The magnetic properties and possible interaction mechanisms between two different hard phases were evaluated by the FORC method, which is hopeful to provide a rudimentary knowledge of the reversal process of the magnetization in the magnets sintered by the dual alloy method.

2. Experiment

Alloys with the stoichiometric composition of $\text{MM}_{14}\text{Fe}_{79.9}\text{B}_{6.1}$ and commercial $\text{Nd}_{13.5}\text{Fe}_{80.5}\text{B}_6$ underwent induction melting, strip-casting, hydrogen decrepitating, and

subsequent jet milling. The powders of $\text{MM}_{14}\text{Fe}_{79.9}\text{B}_{6.1}$ and $\text{Nd}_{13.5}\text{Fe}_{80.5}\text{B}_6$ were denoted as $\text{MM}_2\text{Fe}_{14}\text{B}$ and $\text{Nd}_2\text{Fe}_{14}\text{B}$, respectively. After mixing the powders of $\text{MM}_2\text{Fe}_{14}\text{B}$ and $\text{Nd}_2\text{Fe}_{14}\text{B}$ in the mass ratios of 0:100 (S00), 20:80 (S20), and 30:70 (S30), the mixed powders were aligned and compacted under a magnetic field of 1.8 T and a pressure of ~ 5 MPa in a N_2 -filled glove box, followed by isostatically compacting under a pressure of ~ 160 MPa. The green compacts were sintered for 2 h at 1040 °C in a vacuum, followed by a heat treatment for 2 h at 520 °C. Table 1 shows the atomic ratio of rare earth and compositions of the samples (R represents the total rare earth).

Table 1. Compositions of different samples.

Sample	$(M/(M+N))/\text{wt.}\%$	$(\text{MM}/\text{R})/\text{at.}\%$	$(\text{LaCe}/\text{R})/\text{at.}\%$	Atomic composition
S00				$\text{Nd}_{13.5}\text{Fe}_{80.5}\text{B}_6$
S20	20	20.2	16.2	$\text{La}_{0.79}\text{Ce}_{1.45}\text{Pr}_{0.14}\text{Nd}_{11.22}\text{Fe}_{80.38}\text{B}_{6.02}$
S30	30	30.3	24.3	$\text{La}_{1.18}\text{Ce}_{2.18}\text{Pr}_{0.21}\text{Nd}_{10.08}\text{Fe}_{80.32}\text{B}_{6.03}$

The Curie temperature was determined by Model 4 HF-VSM. The grain alignment and phase constitution were identified by XRD using a Rigaku D/Max-2400 diffractometer with Cu $K\alpha$ radiation. The microstructure was characterized by an XL30 S-FEG scanning electron microscope (SEM). The sample used in measuring the FORC diagram was formed into a cuboid of 0.8 mm \times 0.8 mm \times 3 mm, with the geometrical long axis parallel to the c -axis. The hysteresis loops and the FORCs were measured with a magnetic field applied along the long axis, i.e., the c axis of the sample using a superconducting quantum interference device vibrating sample magnetometer (SQUID VSM, Quantum Design MPMS-3) at the temperature of 300 K.

3. Results and discussion

Figure 1(a) shows the XRD patterns collected on the plane perpendicular to the crystallographic alignment for different compositions. The two different main phases are hard to tell apart from these patterns because the lattice constants of $\text{MM}_2\text{Fe}_{14}\text{B}$ and $\text{Nd}_2\text{Fe}_{14}\text{B}$ are almost the same. No visible secondary phase can be identified in all samples except for the $\text{R}_2\text{Fe}_{14}\text{B}$ phase. There is no obvious difference between different XRD patterns. The extent of c -axis alignment of $\text{Nd}_2\text{Fe}_{14}\text{B}$ grains is characterized via fitting the standard deviation.^[17,18] According to this model, the orientation deviation σ can be related to the ratio of $I_{\text{HKL}}^{\text{Sample}}$ to $I_{\text{HKL}}^{\text{Powder}}$,^[19]

$$\frac{I_{\text{HKL}}^{\text{Sample}}}{I_{\text{HKL}}^{\text{Powder}}} = A \times \exp\left(-\frac{\phi^2}{2\sigma^2}\right), \quad (1)$$

where σ is the orientation deviation of $\text{Nd}_2\text{Fe}_{14}\text{B}$ grains, ϕ is the angle between the normal of the (HKL) plane and the c -axis, $I_{\text{HKL}}^{\text{Sample}}$ is the intensity of diffraction peaks of the samples, $I_{\text{HKL}}^{\text{Powder}}$ is the intensity of diffraction peaks of the ideally

isotropic powder taken from the standard PDF card of the $\text{Nd}_2\text{Fe}_{14}\text{B}$ phase (#39-0473), and A is a normalized parameter. The fitted curves of the three samples shown in Fig. 1(b) reveal almost the same standard deviations for S00, S20, and S30 (13.7° , 14.2° , and 14.4° , respectively). As the content of MM increases, there is an inconsiderable effect on the crystallographic alignment of the magnets.

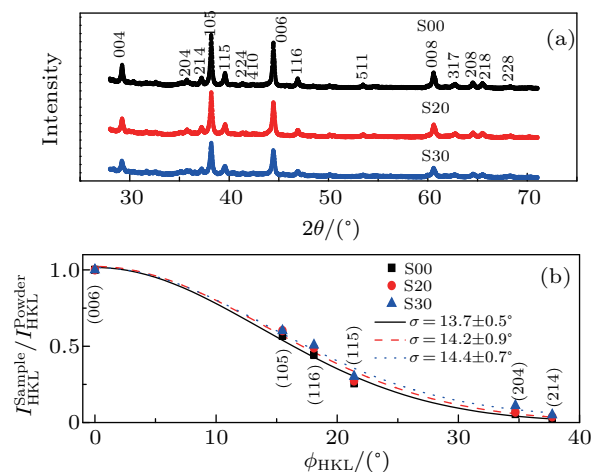


Fig. 1. (color online) (a) XRD profiles and (b) Gaussian fitted curves of orientation deviation of S00, S20, and S30 samples.

The typical SEM-back scattered images of the surfaces are shown in Fig. 2, and the average size of the grains is about 5 μm . The black and white contrasts correspond to the grains and grain boundary phases, respectively. For the S00 magnet (Fig. 2(a)), the grain boundaries are distinct between adjacent grains, and a small amount of grains amalgamate with each other. For the MM partially substituted Nd-Fe-B magnets (Figs. 2(b) and 2(c)), the volume fraction of the intergranular R-rich phase increases slightly. However, it mostly

gathers at the triple junctions, and most of the grain boundary phases cannot be distinguished, indicating that in the local region the grains are close to each other. Such a feature could decrease the coercivity of the magnets since short-range exchange coupling may exist in such local grains. With the increase of the MM content, the number of tiny holes, where reverse magnetic domains primarily form during demagnetization, increases gradually close to the grain boundaries, which indicates that the fluidity between the main phase and the R-rich phase is poor.

In order to determine the magnetic component of the MM partially substituted Nd-Fe-B sintered magnets, the temperature dependent magnetization ($M-T$) was measured with an applied magnetic field of 100 Oe. Figure 3 shows the $M-T$ curves. The dM/dT plots, which are used to determine the Curie temperature of the magnets, are displayed in Fig. 3(b). There is only one Curie temperature of $T_C = 585.2$ K for the S00 magnet. The three minima in the dM/dT versus T curve (Fig. 3(b)) for the S20 and S30 magnets correspond to three different magnetic components. For the convenience of the following description, the Curie temperatures are denoted as

T_{C1} , T_{C2} , and T_{C3} , respectively and summarized in Table. 2. With the content of $MM_2Fe_{14}B$ increasing from 20 wt.% to 30 wt.%, T_{C1} , T_{C2} , and T_{C3} decrease from 509.4 K, 565 K, and 573.2 K to 508.8 K, 555.2 K, and 568.8 K, respectively. Since the Curie temperature of $R_2Fe_{14}B$ magnets is heavily dependent on the relative content of rare earth elements and the T_C of the magnet decreases with increasing Ce/La content, the MM partially substituted Nd-Fe-B magnets contain three types of components with different Ce/La concentrations. It can also be concluded that the magnetic components corresponding to T_{C1} and T_{C3} are similar to $MM_2Fe_{14}B$ and $Nd_2Fe_{14}B$, respectively. It indicates that the initial two different main phases diffused seriously into each other during the sintering process. T_{C1} is the Curie temperature of the initial main phase that contains more LaCe, while T_{C3} corresponds to the initial main phase that contains more Pr/Nd, and T_{C2} corresponds to the new magnetic component formed during the sintering process. Due to the different contents of rare earth elements in the grains of $MM_2Fe_{14}B$ and $Nd_2Fe_{14}B$, the atoms inside inevitably diffuse into each other, which results in magnets with multiple main phases instead of dual main phases.

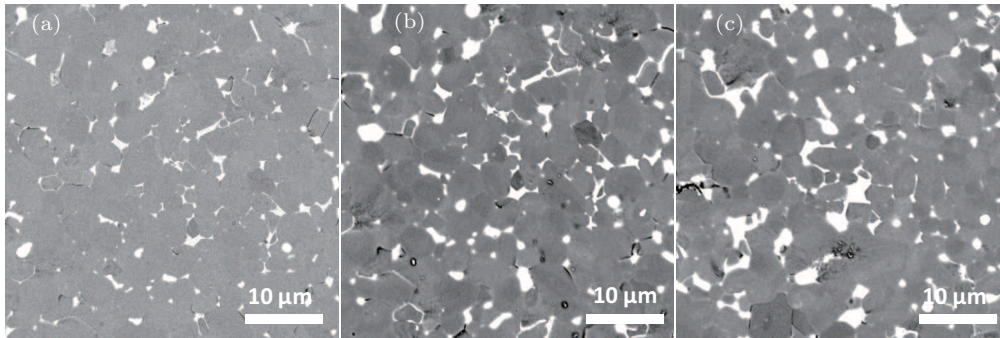


Fig. 2. SEM-back scattered micrographs of the sintered magnets (a) S00, (b) S20, and (c) S30.

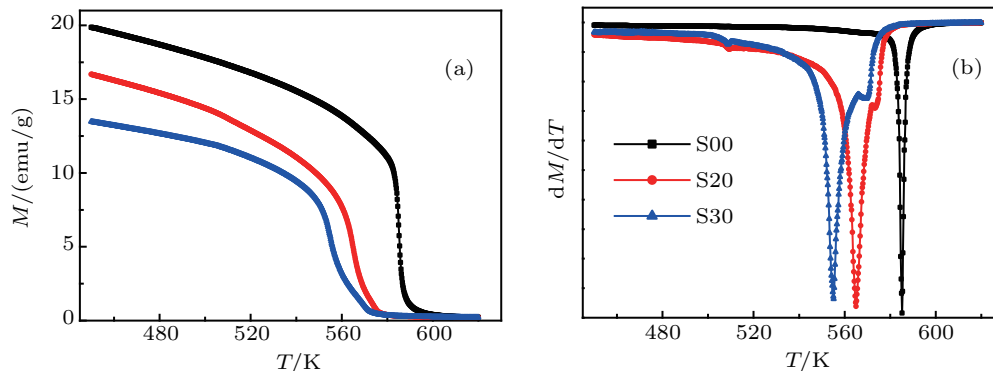


Fig. 3. (color online) Temperature dependence of (a) magnetization and (b) dM/dT of the sintered magnets.

Table 2. Curie temperatures of the sintered magnets.

Sample	T_{C1}/K	T_{C2}/K	T_{C3}/K
S00	—	—	585.2
S20	509.4	565	573.2
S30	508.8	555.2	568.8

In order to study the magnetization reversal process, the

FORC technique^[11,12] was employed. As was described in the literature, the FORC measurement starts from magnetization saturation in one direction of the magnets followed by sweeping down the magnetic field to the opposite direction of a field value H_R , from which the measurement of magnetization M goes back to magnetization saturation, recording

a FORC curve. This sequence of measuring a single FORC curve is used for a series of different H_R with even spacing, which cover the major loop from the beginning of the reversal field to the magnetization saturation in the opposite direction, and a family of FORCs can finally be collected. A mixed second order derivative is utilized to obtain the normalized FORC distribution,^[20–22]

$$\rho(H, H_R) = -\frac{1}{2M_s} \frac{\partial^2 M(H, H_R)}{\partial H_R \partial H}, \quad (2)$$

where M_s is the saturation magnetization of the sample.

This derivative can remove all completely reversible components in the reversal process.^[23] Thus, irreversible magnetization reversal occurs where the derivative is not zero. The derivative ρ , distributed on a two-dimensional contour map in (H, H_R) coordinates, can reflect all irreversible magnetization processes. Each curve corresponding to a specific H_R appears as a straight line parallel to the external field axis on the contour map. This two-dimensional contour map can be displayed in (H_C, H_U) coordinates, where H_C and H_U are the coercive field and the interaction field, respectively.

The FORC contour map gives a useful tool to record the magnetization reversal mechanism of the irreversible magnetization reversal in (H, H_R) coordinates. The one-dimensional distribution of the irreversibility is also very beneficial for a more intuitive recognizing of the magnetization reversal process. This is an integral of the derivative ρ over the external magnetic field H ,^[24]

$$\int \frac{\partial^2 M(H, H_R)}{\partial H_R \partial H} dH = \frac{\partial M(H_R)}{\partial H_R}, \quad (3)$$

and is called the FORC switching field distribution (FORC-SFD).

The effect of MM content variation to the reversal mechanisms is derived from the analysis of a series of FORCs (Figs. 4(a)–4(c)) and the corresponding FORC distributions (calculated using Eq. (2), shown in Figs. 4(d)–4(f)). A small step in the second quadrant of the FORCs is owing to the presence of uncoupled soft magnetic phase grains, such as surface grains.^[15,16] Besides S00, the two-dimensional contour plots of the other two samples show two peaks, except for another one near the coordinate origin, which indicates that the magnets have two distinctly different magnetization components, corresponding to two different main phases, although three types of magnetic components are confirmed by the curves of the magnetization and dM/dT . The first peak located at the low H corresponds to a relatively softer main phase, and the other peak corresponds to a component that is relatively harder to reverse the magnetization. The positions of the centers of the two peaks are at 750 Oe and 8800 Oe for S20, and 980 Oe and 7740 Oe for S30. The main parts of the FORC diagrams

exhibit two features: (i) a horizontal ridge, which is parallel to the H axis, and (ii) a vertical ridge, which is essentially perpendicular to the H axis. These demonstrate that the domain nucleation and growth are the leading mechanisms in controlling the magnetization reversal processes^[13,25] of the magnets sintered by the dual alloy method. The horizontal ridge indicates that the magnetization reversal of the softer main phase occurs in a larger negative applied field. The nearly simultaneous magnetization reversal of two different magnetization components indicates that a ferromagnetic exchange coupling does exist between them.

The contribution of exchange coupling between the two main phases to the magnetization reversal is also reflected in the asymmetric FORC-SFD (Eq. (3)) in Figs. 4(g)–4(i), which shows a small bump below the coercivity field. This asymmetry is due to the magnetization reversal of the softer main phase occurring before that of the hard phase components. With the increase of the MM content, the main distribution of FORC-SFD is more decentralized on the external field (shown in Figs. 4(g)–4(i)), which indicates that the magnetization reversal process is more inconsistent. The FORC-SFD of S30 shows two peaks near its coercivity, which indicates the relatively low exchange coupling between two main phases in this sample. In addition, a small peak appears near the coordinate origin in the FORC distribution, indicating the existence of some uncoupled soft magnetic phase. The results can also be found in the FORCs with a small step in the second quadrant, and a small protuberance near the zero field in the FORC-SFD.

Grains in sintered magnets exhibit a mutually consistent process of magnetization reversal due to the existence of exchange coupling between different main phases. To qualitatively identify the exchange coupling effect between two main hard phases, a Henkel plot, which is defined as $\delta m = [M_d(H) + 2M_r(H)]/M_r - 1$,^[26,27] is employed. Here $M_r(H)$ is the remanent magnetization that is obtained by the following operation: a sample with initial AC demagnetized state is magnetized in a magnetic field H , and subsequently the external magnetic field is removed. $M_d(H)$ is the remanent magnetization of the demagnetization process, which is obtained by firstly magnetizing the sample to saturation in a certain direction, then applying magnetic field H in the opposite direction, and finally removing it. Generally speaking, the exchange coupling dominates when the value of δm is positive. Otherwise, the dipole interaction plays a leading role. The dependence of δm on the external magnetic is shown in Fig. 5 at the temperature of 300 K for all samples. Each plot of δm has a positive peak near the coercivity. With the increasing extent of the MM, the maximum value of δm gradually decreases. It demonstrates that the inconsistent process of magnetization reversal in the sintered magnets with several magnetic com-

ponents is caused by poor exchange coupling between different main phases with the same degree of grain alignment in the samples (Fig. 1(b)). A more obvious trough appears on each plot of δm , which indicates that the dipole interaction

also plays a very important role in the reversal of magnetization. The weak exchange coupling and the increasing of the dipole interaction make the magnetization reversal process of the sintered magnets containing MM more dispersed.

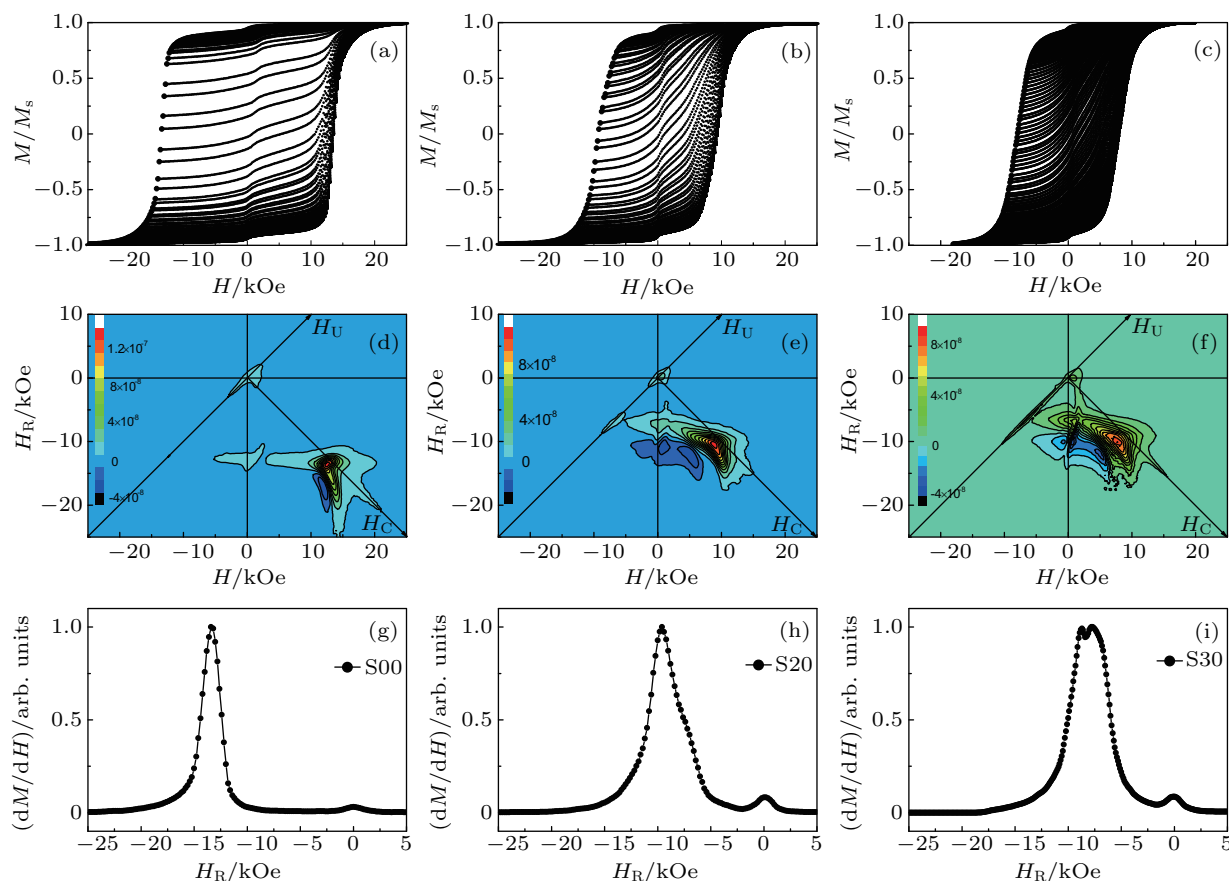


Fig. 4. (color online) Families of FORCs, FORC distributions, and SFDs for S00, S20, S30. The first point of each reversal curve in panel (a)–(c) is shown by a black dot. (d)–(f) The corresponding FORC distributions shown as contour plots. (g)–(i) The FORC-SFDs.

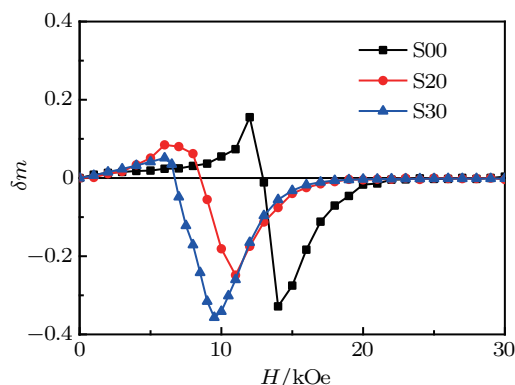


Fig. 5. (color online) The δm curves of the samples.

4. Conclusion

The MM substituted Nd–Fe–B magnets sintered by the dual alloy method are fabricated. As the content of the MM increases, the crystallographic alignment of the magnets stays almost the same. The distribution of two kinds of main phase grains remains substantially unchanged, but the grain bound-

ary environment deteriorates slightly. The non-uniform magnetization reversal in the sintered magnets with several magnetic components is caused by poor exchange coupling between different main phases with the same degree of the grain alignment in the samples. Due to the diffusion between the adjacent grains, the MM substituted Nd–Fe–B magnets contain three types of magnetic components. Moreover, the analysis of the FORC diagram demonstrates that there are two major reversal components, corresponding to the two different main phases. The study also demonstrates that the grains reverse by a domain nucleation and growth mechanism.

References

- [1] Jiles D C 2003 *Acta Mater.* **51** 5907
- [2] Jones N 2011 *Nature* **472** 22
- [3] Herbst J F, Meyer M S and Pinkerton F E 2012 *J. Appl. Phys.* **111** 07A718
- [4] Pathak A K, Khan M, Gschneidner K A, McCallum R W, Zhou L, Sun K, Kramer M J and Pecharsky V K 2016 *Acta Mater.* **103** 211
- [5] Herbst J F 1991 *Rev. Mod. Phys.* **63** 819
- [6] Shang R X, Xiong J F, Liu D, Zuo S L, Zhao X, Li R, Zuo W L, Zhao T Y, Chen R J, Sun J R and Shen B G 2017 *Chin. Phys. B* **26** 057502

- [7] Zhu M G, Han R, Li W, Huang S L, Zheng D W, Song L W and Shi X N 2015 *IEEE Trans. Magn.* **51** 11
- [8] Ma T Y, Yan M, Wu K Y, Wu B, Liu X L, Wang X J, Qian Z Y, Wu C and Xia W X 2018 *Acta Mater.* **142** 18
- [9] Zhou B B, Li X B, Cao X J, Yan G L and Yan A R 2016 *Chin. Phys. B* **25** 117504
- [10] Li Z B, Zhang M, Shen B G and Sun J R 2013 *Appl. Phys. Lett.* **102** 102405
- [11] Hono K and Sepehri-Amin H 2012 *Scr. Mater.* **67** 530
- [12] Ma T Y, Wu B, Zhang Y J, Jin J Y, Wu K Y, Tao S, Xia W X and Yan M 2017 *J. Alloys Compd.* **721** 1
- [13] Dumas R K, Li C P, Roshchin I V, Schuller I K and Liu K 2007 *Phys. Rev. B* **75** 134405
- [14] Davies J E, Hellwig O, Fullerton E E, Denbeaux G, Kortright J B and Liu K 2004 *Phys. Rev. B* **70** 224434
- [15] Davies J E, Hellwig O, Fullerton E E, Jiang J S, Bader S D, Zimanyi G T and Liu K 2005 *Appl. Phys. Lett.* **86** 262503
- [16] Mayergoyz I D and Friedmann G 1988 *IEEE Trans. Magn.* **24** 212
- [17] Givord D, Lienard A, DeLaBathie R P, Tenaud P and Viadieu T 1985 *J. Phys. Colloq.* **46** 313
- [18] Tenaud P, Chamberod A and Vanoni F 1987 *Solid State Commun.* **63** 303
- [19] Zhang T Q, Chen F G, Wang J, Zhang L T, Zou Z Q, Wang Z H, Lu F X and Hu B P 2016 *Acta Mater.* **118** 374
- [20] Pike C R, Roberts A P and Verosub K L 1999 *J. Appl. Phys.* **85** 6660
- [21] Katzgraber H G, Pazmandi F, Pike C R, Liu K, Scalettar R T, Verosub K L and Zimanyi G T 2002 *Phys. Rev. Lett.* **89** 257202
- [22] Liu W and Zhang Z D 2017 *Chin. Phys. B* **26** 117502
- [23] Olamit J, Liu K, Li Z P and Schuller I K 2007 *Appl. Phys. Lett.* **90** 032510
- [24] Dumas R K, Fang Y, Kirby B J, Zha C, Bonanni V, Nogues J and Akerman J 2011 *Phys. Rev. B* **84** 054434
- [25] Davies J E, Hellwig O, Fullerton E E, Winklhofer M, Shull R D and Liu K 2009 *Appl. Phys. Lett.* **95** 022505
- [26] Henkel O 1964 *Phys. Status Solidi* **7** 919
- [27] Kelly P E, O'Grady K, Mayo P I and Chantrell R W 1989 *IEEE Trans. Magn.* **25** 3881